

Image processing and analysis in a dual-modality optoacoustic/ultrasonic system for breast cancer diagnosis

Vyacheslav Nadvoretzkiy*, Sergey Ermilov, Hans-Peter Brecht, Richard Su, Alexander Oraevsky

TomoWave Laboratories Inc., 675 Bering Dr., Suite 575, Houston, TX 77057

ABSTRACT

Coregistered optoacoustic (OA) and ultrasound (US) images obtained using a dual modality optoacoustic/ultrasonic breast imaging system are used together for enhanced diagnostic capabilities in comparison to each individual technology. Therefore, an operator-independent delineation of diagnostically relevant objects (in our case breast tumors) with subsequent automatic analysis of image features is required. We developed the following procedure: 1) Image filtering is implemented on a US image to minimize speckle noise and simultaneously preserve the sharpness of the boundaries of the extended objects; 2) Boundaries of the objects of interest are automatically delineated starting with an initial guess made by an operator; 3) Both US and OA images are analyzed using the detected boundaries (contrast, boundary sharpness, homogeneity of the objects and background, boundary morphology parameters are calculated). Calculated image characteristics can be used for statistically independent evaluation of structural information (US data) and vascularization (OA data) of the studied breast tissues. Operator-independent delineation of the objects of interest (e.g. tumors and blood vessels) is essential in clinical OA spectroscopy (using multiple laser wavelengths to quantify concentrations of particular tissue chromophores, such as oxy- and deoxy- hemoglobin, water, and lipids). Another potential application of the suggested image analysis algorithm could be in OA imaging system design, when system performance should be evaluated in terms of quality of the images reconstructed from the well-defined objects of interest. The discussed principles of image analysis are illustrated by using real clinical US and OA data.

Keywords: Ultrasonic imaging, optoacoustic tomography, boundary detection, tumor morphology.

1. INTRODUCTION

We developed dual modality breast cancer imaging system with a commercial handheld ultrasonic probe^{1,2}. This new laser optoacoustic/ultrasonic imaging system (LOUIS) combines ultrasound tissue visualization with optoacoustic imaging of blood distribution. Ultrasonic mode allows good visualization of the possible tumor since its acoustic properties are known to be different from the normal breast tissue, and the tumor shape somehow correlates with its malignancy³.

Optical absorption is closely associated with hemoglobin concentration and oxygen saturation⁴⁻⁶. Breast tumors have increased blood concentration due to their own microvasculature^{7,8}, so optoacoustic imaging provides functional information directly correlated with cancer angiogenesis.

Tumor boundaries may or may not coincide in reconstructed images for both modalities respectively. Therefore, it is particularly important to have a standardized method of boundary delineation for further image analysis. In this study we propose a semi-automated algorithm of boundary recognition as well as the set of parameters to quantify two image domains (inside and outside of the boundary) as well as the boundary morphology.

* vv@tomowave.com; phone +1 (713) 366-3387; www.tomowave.com

2. MATERIALS AND METHODS

The major system components and principles of operation were described in our previous publications².

We use the image processing protocol that can be applied in the same way to the images obtained regardless of the modality used. The algorithms were coded in Matlab (MathWorks Inc.). First we apply the US image filtering to smooth the background speckle noise. Then operator draws the initial guess boundary around the region of interest (ROI) since a fully automated boundary detection approach is not possible on images that contain irrelevant objects and/or artifacts. The initial boundary is drawn on US image assuming it provides better visualization of tumor location due to strong specular reflections from its anterior and posterior boundaries. Automated boundary detection algorithm corrects the initial boundary by snapping it to the points of the highest gradient in the neighborhood of the initial guess. Parameters that define tumor size and location, such as perimeter, area, center of masses, are calculated for the detected boundary. Contrast and sharpness of ROI are calculated based on the approach described in our previous work². Boundary morphology is estimated in a set of parameters based on its shape (radial distance mean, radial distance standard deviation, eccentricity, compactness, local and global roughness).

3. RESULTS

3.1 Image filtering

Automatic image segmentation and boundary recognition techniques cannot be directly applied to the OA or US images. The images may contain irrelevant objects and artifacts as well as background speckle noise. Nonlinear diffusion filtering is one of the most promising approaches since it smooths the image while retains the relatively sharp edges of extended objects⁹. We used the custom-made Matlab function based on adaptive diffusion image filtering with diffusivity function which corresponds to backward diffusion (edge enhancing total variance flow)¹⁰. Fig. 1 illustrates the effect of filtering on the outcome of the boundary detection.

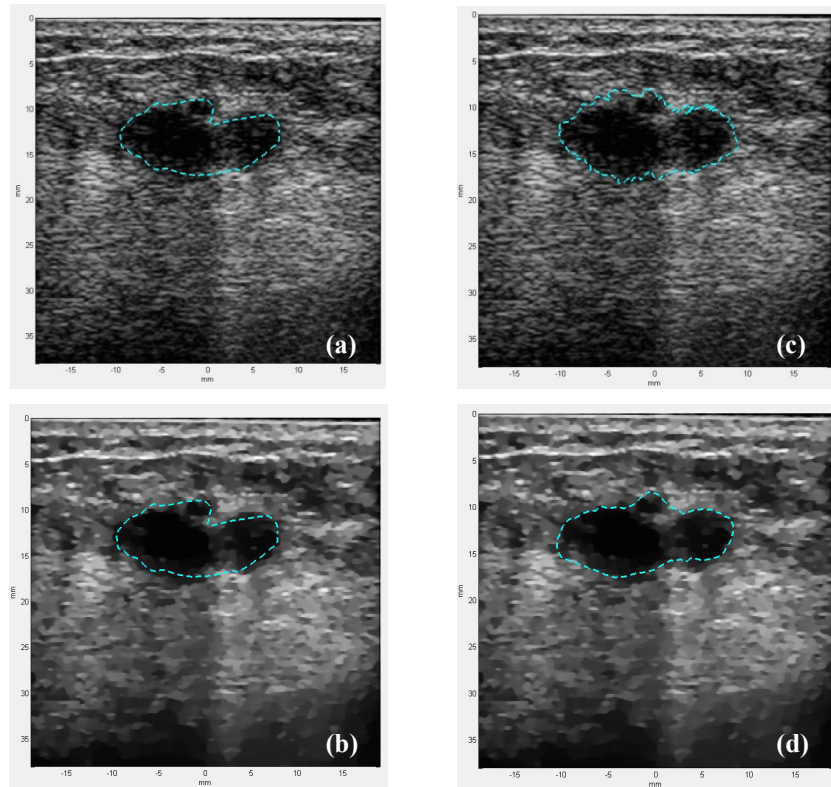


Figure 1: a – original image with initial guess boundary; b – filtered image with initial guess boundary; c – original image with autodetected boundary; d – filtered image with autodetected boundary

3.2 Boundary detection

Operator draws an initial guess boundary delineating the potential ROI (Figure 1b). Automated boundary recognition function converts it to the ‘true’ boundary based on user-defined settings, which include the distance from the initial boundary (local neighborhood), gradient threshold, smoothing and magnet coefficients.

The gradient magnitude and direction are calculated for the filtered US image using Sharr operator. Then each group of five consecutive pixels of the initial boundary is fit using the linear regression. Each particular fitted line represents a tangent to the central (i.e. the 3rd one) point of the corresponding group. For each pixel of the boundary the norm is evaluated as a line that is orthogonal to the corresponding tangent. The projections of the image intensity gradient on each norm are calculated and weighted by the magnet coefficients (see below). For the user-specified distance from the initial boundary, the point with the maximum absolute value of the weighted gradient projection is found, and this point is set as the new boundary point. Next, some of the new boundary points could be eliminated if their weighted gradient projections are below the specified threshold. Then the boundary is smoothed with Savitzky-Golay filter and the possible gaps are filled by linear interpolation. After that the boundary recognition process is iteratively repeated with the new boundary as an initial guess until the overall boundary sharpness remains unchanged or decreases. The overall boundary sharpness is defined as a sum of gradient magnitudes at all points of the boundary.

The magnet coefficient (Eq. 1) is a tradeoff between the human and machine perception of the object boundaries. If it is anticipated that the ‘true’ boundary is close to the initial one (based on the operator’s expertise, for instance), the magnet parameter M should be set to 1. If the ‘true’ boundary can be at any distance within the predefined range from the initial one, than the magnet parameter should be set to 0. The weight coefficient w is then defined as a function of the distance from the initial boundary x as follows:

$$w(x) = 1 + M \cdot \left(\cos\left(\frac{\pi}{2n} x\right) - 1 \right) \quad (1)$$

where x is the distance from the central point of the initial boundary (ranged from $-n$ to n), and n is defined by the size of the local boundary neighborhood. Fig. 2 illustrates weight coefficient function for different magnet parameters.

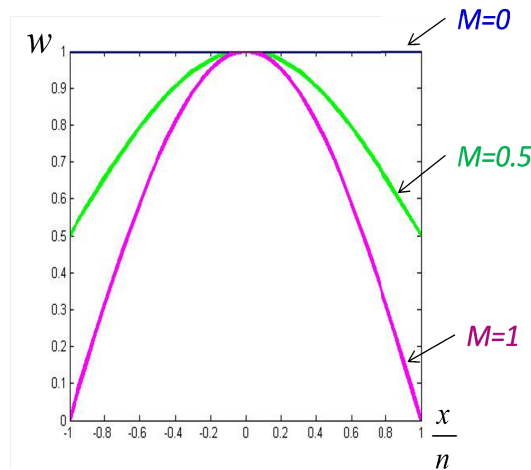


Figure 2: Magnet weight coefficient as a function of relative distance from the boundary for different magnet parameters.

3.3 Boundary morphology parameters

We developed the set of parameters related to the morphology of the boundary. This set includes eccentricity, compactness, global and local roughness, radial distance mean, and radial distance standard deviation. We use the following definitions: x_i, y_i – coordinates of the i -th ROI boundary point; X_0, Y_0 – coordinates of ROI center of masses; r_i – radial distance of the i -th ROI boundary point (with respect to the ROI center of masses); \bar{r} – average of $\{r_i\}$; X_{BFC}, Y_{BFC} – coordinates of the center of the circle, which is best-fit to the ROI boundary; R_{BFC} – its radius; P – perimeter of ROI; A – area of ROI; N – number of ROI boundary points.

Then we can define the following parameters:

$$Eccentricity = \sqrt{\frac{\lambda_1}{\lambda_2}} \quad (2)$$

where λ_1 and λ_2 are the eigenvalues of the following matrix:

$$\begin{bmatrix} \sum_{i=1}^N (x_i - X_0)^2 & \sum_{i=1}^N (x_i - X_0)(y_i - Y_0) \\ \sum_{i=1}^N (x_i - X_0)(y_i - Y_0) & \sum_{i=1}^N (y_i - Y_0)^2 \end{bmatrix}$$

$$Compactness = \frac{P^2}{4\pi A} \quad (3)$$

$$Global_Roughness = \frac{\left[\frac{1}{N} \sum_{i=1}^N (r_i - \bar{r})^4 \right]^{\frac{1}{4}} - \left[\frac{1}{N} \sum_{i=1}^N (r_i - \bar{r})^2 \right]^{\frac{1}{2}}}{\bar{r}} \quad (4)$$

We use the following algorithm to calculate the local roughness parameter:

- Calculate the ‘snake segment’ – N points constituting the first millimeter of a boundary;
- Determine tangent line to this segment and calculate its slope S_i ;
- Determine curvature of this segment as $C = 1/R_{BFC(N)}$; where $R_{BFC(N)}$ – radius of the circle, which is best-fit to the N points of the “snake segment”;
- Apply that procedure to all consecutive segments of the boundary for all points (like a snake) and determine the array of C and S_i values;
- Calculate the differentials of those arrays, since we’re interested in certain boundary regions where the significant change of tangent slope or curvature takes place;
- Normalize the differentials to [0; 1] interval and determine how many boundary points have values over 0.5: N_1 (for tangent slopes) and N_2 (for curvatures);
- Calculate the local boundary roughness as $(N_1 + N_2) / (N - N_1 - N_2)$.

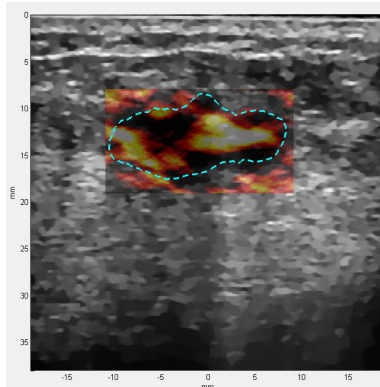


Figure 3: Dual-modality image of the breast tumor and the detected ROI boundary.

Fig. 3 shows the part of the interface of the LOUIS program with a reconstructed OA image of a breast tumor on the top of the co-registered US image and the detected boundary of the tumor. Functional and morphological parameters for that image are displayed on Fig. 4.



Figure 4: Functional and morphological parameters calculated for the breast tumor.

4. CONCLUSIONS

The image processing protocol has been developed to analyze the US and OA clinical images to enhance the diagnostics of breast cancer. Standardized procedure includes delineation of ROI containing breast tumor with the following quantification based on its intensity in both modalities as well as its shape. Preliminary studies showed that computer-assisted boundary recognition algorithm produce good results in localizing the tumor.

The future prospects are to apply the developed protocol to the set of clinical OA and US images for blind processing. The goal of this study will be to delineate the tumor boundaries and calculate the tumor functional and morphological parameters, and to apply the relevant statistical tests to find of there any statistically significant difference between the malignant and benign tumors.

ACKNOWLEDGMENTS

This work was partially supported by Seno Medical Instruments (San Antonio, Texas).

REFERENCES

- [1] Fronheiser, M. P., Ermilov, S. A., Brecht, H. P., Conjusteau, A., Su, R., Mehta, K. and Oraevsky, A. A., "Real-time optoacoustic monitoring and three-dimensional mapping of a human arm vasculature," *Journal of biomedical optics* 15(2), 021305 (2010).
- [2] Ermilov, S. A., Fronheiser, M. P., Nadvoretzky, V., Brecht, H.-P., Su, R., Conjusteau, A., Mehta, K., Otto, P. and Oraevsky, A. A., "Real-time optoacoustic imaging of breast cancer using an interleaved two-laser imaging system coregistered with ultrasound," *Proceedings SPIE 7564*, 75641W (2010).

- [3] Wu, W. J. and Moon, W. K., "Ultrasound breast tumor image computer-aided diagnosis with texture and morphological features," *Academic radiology* 15(7), 873-880 (2008).
- [4] Ntziachristos, V. and Chance, B., "Probing physiology and molecular function using optical imaging: applications to breast cancer," *Breast Cancer Res* 3(1), 41-46 (2001).
- [5] Pogue, B. W., Jiang, S., Dehghani, H., Kogel, C., Soho, S., Srinivasan, S., Song, X., Tosteson, T. D., Poplack, S. P. and Paulsen, K. D., "Characterization of hemoglobin, water, and NIR scattering in breast tissue: analysis of intersubject variability and menstrual cycle changes," *Journal of biomedical optics* 9(3), 541-552 (2004).
- [6] Alacam, B., Yazici, B., Chance, B. and Nioka, S., "Characterization of breast tumors with NIR methods using optical indices," *Conf Proc IEEE Eng Med Biol Soc* 2007, 5186-5189 (2007).
- [7] Rice, A. and Quinn, C. M., "Angiogenesis, thrombospondin, and ductal carcinoma in situ of the breast," *Journal of clinical pathology* 55(8), 569-574 (2002).
- [8] Naumov, G. N., Akslen, L. A. and Folkman, J., "Role of angiogenesis in human tumor dormancy: animal models of the angiogenic switch," *Cell cycle (Georgetown, Tex)* 5(16), 1779-1787 (2006).
- [9] Perona P. and Malik J., Scale space and edge detection using anisotropic diffusion, *IEEE Transactions on Pattern Analysis and Machine Intelligence* 12 (1990), 629-639.
- [10] Weickert J., "Applications of nonlinear diffusion in image processing and computer vision", *Acta Math. Univ. Comenianae*, Vol. LXX, 1(2001), pp. 33-50.